V International Conference on Simulation for Additive Manufacturing
Sim-AM 2025
F. Auricchio, M. Carraturo and S. Morganti (Eds)

TOPOLOGY OPTIMIZATION WITH LIMITS ON JOINT LOADS

JOHANNES SOIKA*, JAKOB SCHENK† AND MARKUS ZIMMERMANN*

*Laboratory for Product Development and Lightweight Design
Technical University of Munich
Boltzmannstr. 15, 85748 Garching bei München, Germany
e-mail: johannes.soika@tum.de, web page: www.mec.ed.tum.de/en/lpl/home/ /

†AUDI AG
85057 Ingolstadt, Germany

Key words: connection elements, topology optimization, bolted joints, Design for Additive Manufacturing (DfAM)

Abstract. Additive manufacturing (AM) and topology optimization (TO) together enable complex, lightweight components tailored to specific performance targets. In this setting, bolted joints remain indispensable, as for assembly, maintenance, and overcoming AM build-volume limits, and they often become the critical regions of the structure. In connections with multiple bolted joints, loads can be distributed across the joints and thus relieve an overloaded connection. Designing a structure that keeps every joint within its limit is difficult, especially when normal and shear forces act simultaneously. Prior studies have integrated connection elements into topology optimization. However, explicit constraints on joint loads under combined loading have received limited attention.
This work includes a joint load constraint in topology optimization for bolted joints. Bolts are implicitly represented as in the VDI 2230 model class I. The required preload is computed from internal forces at the interface, and is limited by the allowable preload of the bolt. Adjoint sensitivities of the joint load constraint are derived for efficient gradient-based optimization. The constraint is implemented in a simple 2D TO code in MATLAB. Two 2D examples, a cantilever and an engine transmission crossmember, demonstrate substantial reductions in joint loads and allow a reduction in the number of bolts while keeping all joints below their limits. The constraint steers designs to reduce shear loads at the joints, with an expected trade-off of increased compliance. The formulation is computationally inexpensive (one additional adjoint solve per constraint) and is readily extendable to 3D and to models with explicit preload. Further, it can be used to synthesize compliant mechanisms.

1 INTRODUCTION

Topology optimization (TO) is a widely applied method for structural design across many sectors, including aerospace [1, 2], automotive [3, 4], and other engineering disciplines [5, 6]. Since its origins in the late 1980s [7], TO has matured into an efficient engineering tool with many practical applications [8]. The rise of additive manufacturing (AM) has accelerated this trend, because the complex, non-intuitive geometries produced by TO can be fabricated at scale [9]. Nevertheless, translating optimized layouts into manufacturable, reliable hardware remains a challenge [10].

Connection elements play a central role in many engineering applications [11]. Even with high functional integration, joints are indispensable, for example, to bridge limited AM build volumes, to

enable modular assembly, or to allow maintenance and replacement. At the same time, joints are typical critical points for failure and thus often over-dimensioned. When TO pushes components near performance limits, a reliable and efficient treatment of joints becomes essential.
Among joining methods, bolted joints are especially relevant: they carry high loads, are well standardized, and enable non-destructive disassembly. Several approaches have been proposed to represent bolted joints in TO [12, 13, 14, 15, 16]. A common simplification is to idealize joints with infinite strength, e.g., via fixed nodes in the finite element (FE) model. Another frequent abstraction is a beam or spring representation of the joint [14], which captures stiffness effects but not joint failure. Such assumptions can be exploited by the optimizer, leading to concentrated load paths and potential joint overload. A more robust alternative is to impose explicit joint load limits. Chickermance et al. [15] optimize joint layout subject to load limits within a fixed topology. Zhu et al. [16] formulate multi-fastener loads as explicit constraints in TO and model joints as short beams while constraining shear, but other load modes are not considered.

Building on this foundation, a method is developed to include joint load constraints for combined loading in TO. The focus lies on bolted joints modeled according to VDI 2230 model class I [17], meaning the bolt is not explicitly modeled. Instead, normal and shear loads at the interface are considered. Sensitivities are obtained via the adjoint method. The implementation is carried out in MATLAB using a modified 88-line framework [18]. Furthermore, the potential of the method to reduce the number of joints while respecting load limits is examined.

This paper is structured as follows. Section 2 introduces the joint representation in the FE model and the failure of the joint. Section 3 gives the optimization problem and derives the sensitivities of the constraint function. Section 4 presents numerical examples. Section 5 discusses key observations and limitations, followed by a conclusion and outlook in Section 6.

2 MODELLING OF A BOLTED JOINT

This section summarizes the relevant loading scenarios for bolted joints and the FE modeling choices that enable an adequate treatment of joints in TO. Different modeling strategies exist in the literature [11, 12, 13, 14, 16, 19]. These approaches differ in how the bolt, and the contact interface are represented and in whether preload is included.

2.1 Finite element representation of a joint

The FE representation of a joint effects both accuracy and cost. More detailed models are more realistic but also more expensive. VDI 2230 Part 2 [17] distinguishes four model classes:
Model class I. The components are modeled as continuous bodies in the clamping area or, for an isolated part, with the interface kinematically fixed. The interface is represented by equivalent load path section forces and moments.
Model class II. The bolt is represented by a tension member, beam, or spring element. Internal bolt forces are available for verification. Contact and preload can be included (e.g., [13, 14, 16]).
Model class III. The bolt is modeled as an equivalent volume with realistic geometry (without thread), permitting preload and contact both in the interface and under the bolt head and nut.
Model class IV. A detailed bolt model including threads and contact on all relevant surfaces.

Figure 1 (a) shows a bolted joint with two clamped components. The quantities $F_{lp,n}$ and $F_{lp,t}$ denote the normal and tangential load path section forces at a given position along the load path toward the joint. Figure 1 (b) shows the free body diagram of the components with section forces and moments at the interface. The terms $F_{cp,n}$ and $F_{cp,t}$ are the normal and tangential (shear) contact

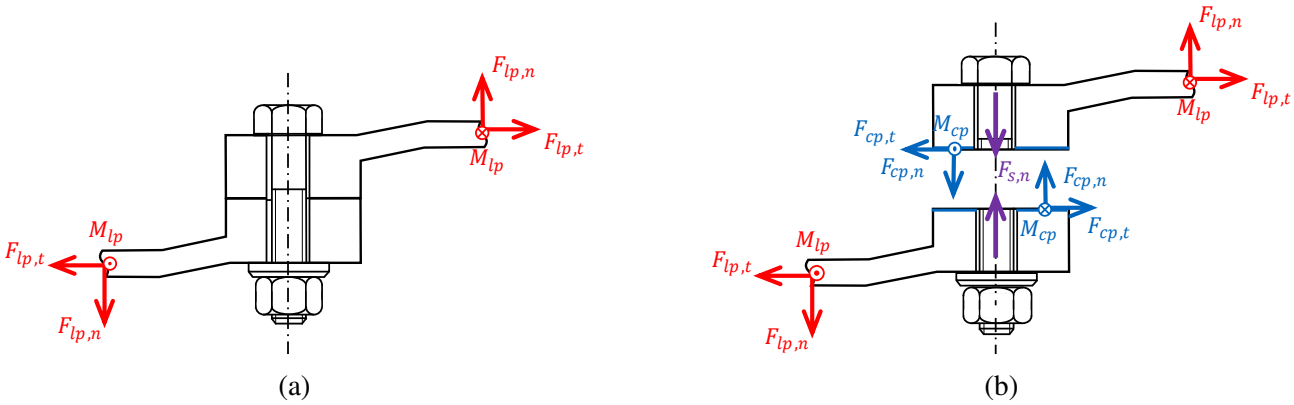

Figure 1: (a) bolted joint with section forces at the load path. (b) free body diagram of the two components with section loads at the contact patch (blue) and the bolt (purple).

patch section forces, and $F_{s,n}$ is the normal bolt force, while the tangential force is taken as zero. For a single component, force equilibrium gives

$$F_{cp,t} = F_{lp,t} \tag{1}$$
$$F_{cp,n} = F_{lp,n} - F_{s,n}. \tag{2}$$

The normal bolt force $F_{s,n}$ depends on the bolt pretension F_M and the load path force normal to the interface $F_{lp,n}$ through the bolt-load factor ϕ. The factor ϕ represents the ratio between contact patch relief and additional joint force under external loading. It depends on the stiffness ratio of the bolt and the surrounding structure. In this study, the bold-load factor is set to $\phi = 0$, a conservative choice that assigns the external load entirely to the loss of interface compression. Loss of preload during service is not considered. Under these assumptions,

$$F_{s,n} = F_{lp,n}\phi + F_M \approx F_M. \tag{3}$$

For model class I, the joint is modeled implicitly. The next section discusses why this approximation is valid. Because $F_{s,n}$ is not present in the FE system, the load path section forces $\mathbf{F}_{lp,k}$ at interface k are used for joint verification. Figure 2 (a) shows the simplified model for the upper component in a more general tensor notation.

In this work model class I is considered. A single component is optimized, and the interface at the joint location is fixed via an Rigid Body Element of Form 2 (RBE2) connection, as in Figure 2 (b). The number of interface nodes depends on the mesh size and the required internal loads. For FE models with nodes of two degrees of freedom, only one node is needed to determine normal and shear forces. However, resolving interface moments requires at least two nodes. For accurate modeling, several nodes are recommended [20].

2.2 Failure of a bolted joint

Bolted joint "failure" can refer to bolt rupture or to interface failure. For highly loaded single bolts, the latter is typically defined as opening (gapping) or sliding [11]. One-sided opening due to bending moments at the interface is not considered in this study. The following requirements prevent failure:

1. To avoid opening: $F_{cp,n} \leq 0$; the contact patch section force must be compressive.

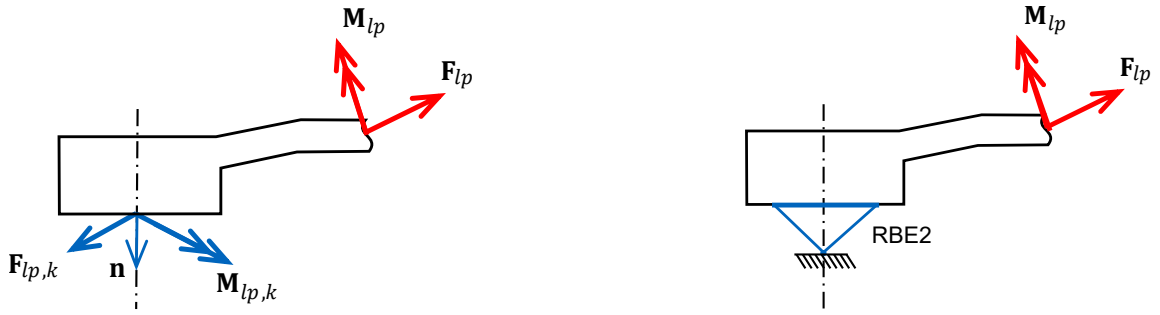

Figure 2: (a) free-body diagram of the clamped part (according to model class I) of the upper component in tensor notation (b) FE representation used in this work. The joint is not modeled explicitly. An RBE2 ties interface nodes, and reaction forces at the interface are used to compute joint loads.

2. To avoid sliding: $F_{cp,n} + \frac{1}{\mu}|F_{cp,t}| \leq 0$; the compressive force at the interface must be sufficient to balance the tangential (shear) force.

3. To avoid bolt rupture: $F_{s,n} \leq F_{M,c}$, where $F_{M,c}$ is the allowable assembly preload including a safety factor against plastic deformation (see VDI 2230 Part 1 [19]).

Requirement 2 implies requirement 1. Substituting equations (2) and (3) into requirement 2 yields

$$F_{lp,n} + \frac{1}{\mu}|F_{lp,s}| \leq F_M. \tag{4}$$

Using (3) and (4) in requirement 3 gives

$$F_{lp,n} + \frac{1}{\mu}|F_{lp,s}| \leq F_{M,c}. \tag{5}$$

In this inequality, all three requirements are considered. Only the load path section forces $\mathbf{F}_{lp,k}$ are needed from the FE system for requirements verification, proving that the model representation as in model class I is sufficient. In vector form, using the notation in Figure 2 (a), equation (5) becomes

$$\mathbf{n}^T\mathbf{F}_{lp,k} + \frac{1}{\mu}|| \left(\mathbf{I} - \mathbf{n}\mathbf{n}^T\right) \mathbf{F}_{lp,k}|| \leq F_{M,c} \tag{6}$$

i.e., the left-hand side combines the signed normal component and a friction-amplified norm of the tangential component of $\mathbf{F}_{lp,k}$ at interface k, with the interface normal $\mathbf{n}$.

3 OPTIMIZATION SETUP

3.1 Optimization problem formulation with joint loads

In practice, the optimization problem is derived from system requirements [21]. Common objectives are minimum mass or minimum compliance, subject to constraints on displacements, stresses, or mass. Here the static compliance l is minimized subject to a mass budget and an additional constraint that limits the joint load. The joint load constraint embodies the allowable preload $F_{M,c}$ of the bolt.

$$\begin{aligned} \min_{\rho(x)} \quad & l \\ \text{s.t.} \quad & m \leq m_0 \\ & g_k \leq 0 \end{aligned} \tag{7}$$

where g_k is the constraint on the joint loads as in equation (8). This equation considers the combination of centrical normal forces and shear forces in equation (6).

$$g_k = \frac{\mathbf{n}^T\mathbf{F}_{lp,k} + \frac{||\mathbf{P}_t\mathbf{F}_{lp,k}||}{\mu}}{F_{M,c}} - 1 \tag{8}$$

For readability, the tangent projector $\mathbf{P}_t$ is introduced as

$$\mathbf{P}_t = \left(\mathbf{I} - \mathbf{n}\mathbf{n}^T\right). \tag{9}$$

The term $\mathbf{n}^T\mathbf{F}_{lp,k}$ in equation (8) captures normal loading (tension increases the required preload, compression reduces it). The term $||\mathbf{P}_t\mathbf{F}_{lp,k}||$ considers the magnitude of the shear forces on the interface.

3.2 Sensitivity analysis of the joint loads

A gradient-based optimization scheme is used. Therefore, first order derivatives of g_k is needed as sensitivity information. The adjoint method is used for the practical derivation of the constraints.
In the following, let ρ_e denote the element density design variable, $\mathbf{q}$ the displacement vector, $\mathbf{K}$ the global stiffness matrix, and $\mathbf{f}$ an external load vector. The derivative of the constraint can be formed as:

$$\frac{\partial g_k}{\partial \rho_e} = \frac{1}{F_{M,c}} \frac{\partial\left(\mathbf{n}^T\mathbf{F}_{lp,k} + \frac{||\mathbf{P}_t\mathbf{F}_{lp,k}||}{\mu}\right)}{\partial \rho_e} \tag{10}$$

$$= \frac{1}{F_{M,c}}\left(\mathbf{n}^T\frac{\partial \mathbf{F}_{lp,k}}{\partial \rho_e} + \frac{1}{\mu}\frac{(\mathbf{P}_t\mathbf{F}_{lp,k})^T}{||\mathbf{P}_t\mathbf{F}_{lp,k}||}\frac{\partial \mathbf{F}_{lp,k}}{\partial \rho_e}\right) \tag{11}$$

Introducing the weighting factor

$$\mathbf{w} = \mathbf{n} + \frac{1}{\mu}\frac{\mathbf{P}_t\mathbf{F}_{lp,k}}{||\mathbf{P}_t\mathbf{F}_{lp,k}||} \tag{12}$$

to obtain the gradient of the constraint as

$$\frac{\partial g_k}{\partial \rho_e} = \frac{1}{F_{M,c}}\mathbf{w}^T\frac{\partial \mathbf{F}_{lp,k}}{\partial \rho_e}. \tag{13}$$

The interface force $\mathbf{F}_{lp,k}$ of interface k can be written as

$$\mathbf{F}_{lp,k} = \mathbf{K}_{lp,k}\mathbf{q} \tag{14}$$

with the stiffness matrix $\mathbf{K}_{lp,k}$. The derivative of the interface force reads

$$\frac{\partial \mathbf{F}_{lp,k}}{\partial \rho_e} = \frac{\partial \mathbf{K}_{lp,k}}{\partial \rho_e}\mathbf{q} + \mathbf{K}_{lp,k}\frac{\partial \mathbf{q}}{\partial \rho_e}. \tag{15}$$

Differentiating the state equation $\mathbf{K}\mathbf{q} = \mathbf{f}$ and multiplying it with an adjoint vector $\boldsymbol{\lambda}$ yields

$$\boldsymbol{\lambda}^T\mathbf{K}\frac{\partial \mathbf{q}}{\partial \rho_e} = \boldsymbol{\lambda}^T\left(\frac{\partial \mathbf{f}}{\partial \rho_e} - \frac{\partial \mathbf{K}}{\partial \rho_e}\mathbf{q}\right). \tag{16}$$

Here, $\partial \mathbf{f}/\partial \rho_e = 0$ because the external load is independent of the design. Choosing $\boldsymbol{\lambda}$ to satisfy

$$\mathbf{K}^T \boldsymbol{\lambda} = -\mathbf{K}_{lp,k}^T \mathbf{w} \tag{17}$$

implies

$$\mathbf{w}^T \mathbf{K}_{lp,k} \frac{\partial \mathbf{q}}{\partial \rho_e} = -\boldsymbol{\lambda}^T \mathbf{K} \frac{\partial \mathbf{q}}{\partial \rho_e}. \tag{18}$$

Substituting equations (15), (16) and (18) into equation (13) obtains the final sensitivity in equation (19) together with the adjoint system (17).

$$\frac{\partial g_k}{\partial \rho_e} = \frac{1}{F_{M,c}} \left(\mathbf{w}^T \frac{\partial \mathbf{K}_{lp,k}}{\partial \rho_e} \mathbf{q} + \boldsymbol{\lambda}^T \frac{\partial \mathbf{K}}{\partial \rho_e} \mathbf{q} \right) \tag{19}$$

4 NUMERICAL EXAMPLES

The method is implemented in a 2D TO code based on the 88-line framework of Andreassen et al. [18]. The FE model uses bilinear quadrilateral elements and linear elasticity, and material interpolation follows the Solid Isotropic Material with Penalization approach. The Method of Moving Asymptotes [22] is used for optimization and a standard density filter is applied. The following examples illustrate the method's behavior under different joint layouts and loading.
For simplicity, $\tilde{g}_k$ is introduced as

$$\tilde{g}_k = \mathbf{n}^T \mathbf{F}_{lp,k} + \frac{||\mathbf{P}_t \mathbf{F}_{lp,k}||}{\mu}. \tag{20}$$

$\tilde{g}_k$ is the numerator of the constraint equation 8 and represents the pretension F_M at which requirement 2 is satisfied with equality. This value can be compared directly with the limit joint load $F_{M,c}$ to verify requirement fulfillment.

4.1 Cantilever example

Setup. The first example is a cantilever beam as in Figure 3. The beam is attached to the left interface by three bolts B_1, B_2 and B_2 and loaded by a force F_1. The problem statement of equation (7) is solved with a mass fraction of 30 %. Two cases are considered: (i) no joint load constraint and (ii) with a joint load constraint and an allowable joint load of $F_{M,c} = 1.5\, F_1$. In the first example, normal effects are isolated by setting a large $\mu = 1000$ such that shear forces are negligible for the constraint. This value for μ is impractical and just for demonstration purposes.

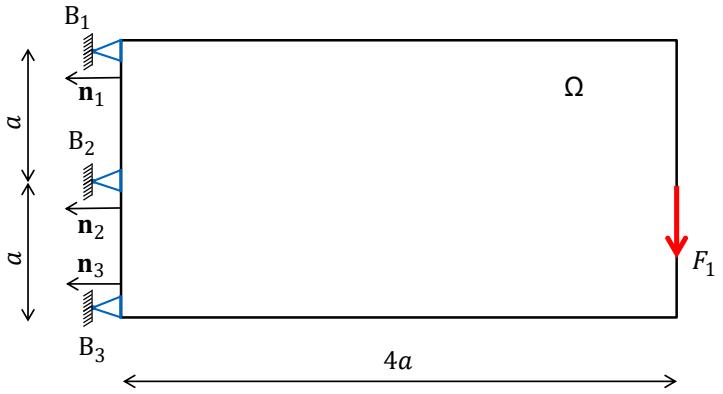

Figure 3: Cantilever benchmark: geometry, boundary conditions, three-bolt interface on the left, and applied load F_1.

Results. Figure 4 compares the topologies. Without the joint constraint (a), the middle bolt (B_2) is not used. With the constraint (b), all three bolts are connected to the structure. Table 1 reports the constraint function $\tilde{g}_k$. In the constrained case, all bolts satisfy $\tilde{g}_k \leq F_{M,c}$. Bolt 1 is critical (tension), while Bolt 3 experiences compression forces at the interface. The negative $\tilde{g}_k$ indicates that this joint is not needed to prevent joint failure at that location.

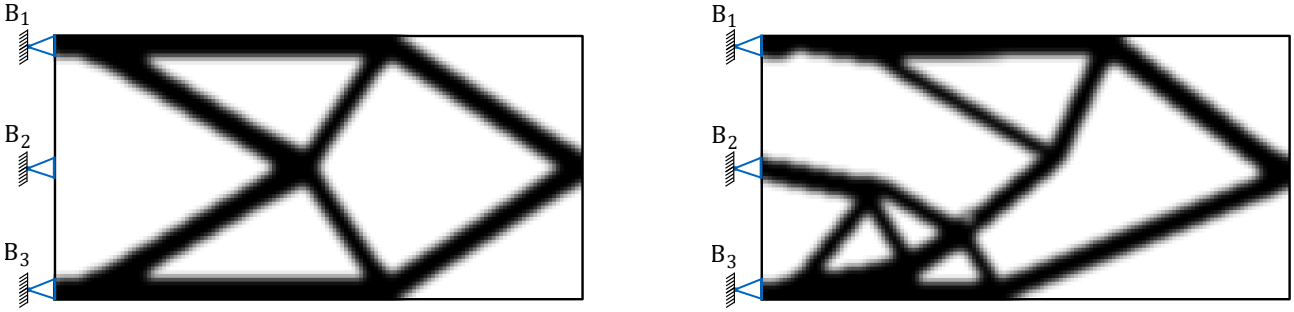

(a) Without joint load constraint.

(b) With joint load constraint $F_{M,c} = 1.5\,F_1$.

Figure 4: Topology-optimized designs for the cantilever example. The constraint promotes load sharing among the three bolts.

Table 1: Cantilever example: constraint function $\tilde{g}_k$ as multiples of F_1, without (i) and with (ii) the joint load constraint.

Setup	$\tilde{g}_1$	$\tilde{g}_2$	$\tilde{g}_3$
(i) inactive	2.0	0	-2.0
(ii) active	1.5	1.0	-2.5

4.2 Transmission crossmember

Setup. The second example is based on a transmission crossmember of an engine. The bolt layout and loading are designed to match typical upper and lower mounting points. For that, the bolt layout

changes: two bolts, B_1 and B_3, at the upper interface and two bolts, B_2 and B_4, at the lower interface. The friction coefficient is set to $\mu = 0.2$, a realistic value for joint interfaces. Both normal and tangential loading effect the joint load constraint $\tilde{g}_k$. Two load cases are considered (Figure 5). The allowable preload remains $F_{M,c} = 1.5\,F_1$, while the mass fraction is now 40 %.

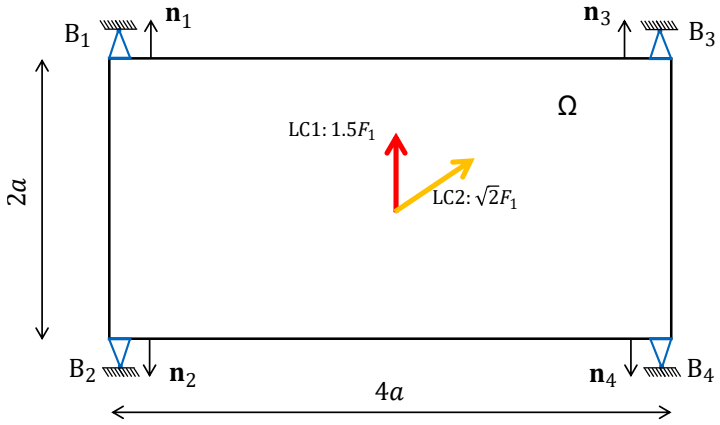

Figure 5: Transmission crossmember benchmark: bolt layout with upper and lower interfaces, unit normals marked at each interface, and two external load cases.

Results. Figure 6 compares the designs without a joint load limit (a) and with a limit (b). In the unconstrained case, the layout forms a nearly straight load path from the central region to the four bolts, concentrating transmission of forces along direct struts. When the limit is enforced, the optimized geometry guides the load into the bolts more normal to the interface, which reduces the shear contribution at each interface. Table 2 lists the required preloads. In the unconstrained case, several bolts exceed $F_{M,c}$, especially in load case 1. With the constraint, all joints satisfy the limit. This results in higher compliance compared with the unconstrained design (last column). The normal forces indicate that compression force at the interface ($F_{lp,n} < 0$) increase in magnitude in bolt B_1 and B_3, while tension ($F_{lp,n} > 0$) decrease in bolts B_2 and B_4. Tangential loads decreased almost everywhere, with the largest reduction in the tension bolts B_2 and B_4.

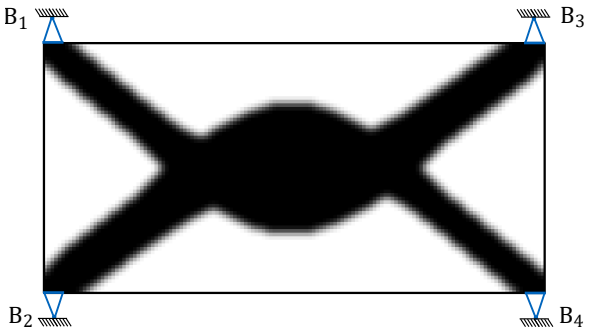

(a) Without joint load constraint.

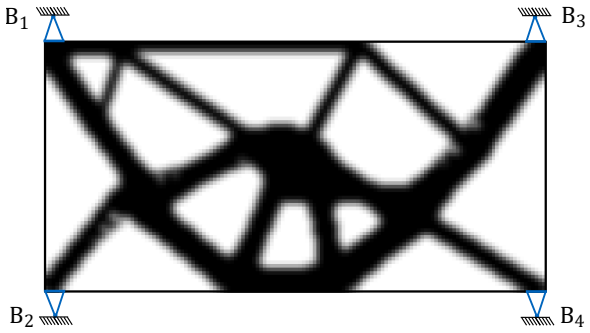

(b) With joint load constraint.

Figure 6: Transmission crossmember: optimized topologies for the two settings. The constraint reduces shear at the joints such that the required preload is below $F_{M,c}$.

Table 2: Transmission crossmember: forces $F_{lp,n}$ and $F_{lp,t}$, the constraint function $\tilde{g}_k$, and compliance for both load cases (LC), without (i) and with (ii) the joint load constraint. All entries are multiples of the external load F_1.

Setup	LC	$\tilde{g}_1$		$\tilde{g}_2$		$\tilde{g}_3$		$\tilde{g}_4$		l [mJ]	
		$F_{lp,n}$	$F_{lp,t}$	$F_{lp,n}$	$F_{lp,t}$	$F_{lp,n}$	$F_{lp,t}$	$F_{lp,n}$	$F_{lp,t}$	-	-
(i) inactive	1	2.13		2.86		2.07		2.76		0.18	
		−0.41	0.51	0.37	0.5	−0.35	−0.48	0.38	−0.48	-	-
	2	0.40		3.44		2.49		0.50		0.11	
		−0.08	0.10	0.44	0.60	−0.42	−0.58	0.07	−0.09	-	-
(ii) active	1	1.06		0.97		1.50		1.50		0.26	
		−0.51	0.31	0.20	0.15	−0.64	−0.43	0.16	−0.27	-	-
	2	0.41		1.50		1.50		0.93		0.22	
		−0.18	−0.12	0.30	−0.24	−0.64	−0.43	−0.12	0.21	-	-

4.3 Reduce number of joints

Setup. In this setup, bolt B_3 from the previous setup in Figure 3 is removed, while keeping the same load cases and limits. With this setup, the reduction of joints is investigated.

Results. Figure 7 (a) shows the optimized structure. All remaining joints satisfy the limit. Figure 7 (b) plots the deformed shape with external and load path forces at the interface for load case 2. Vertical arrows pointing towards the interface indicate compression. Notably, Bolt 2 provides compression at the interface even though the external force pulls away, indicating that a compliant mechanism is obtained. The design behaves partly as a compliant mechanism to meet the joint load constraint. The mechanisms are created by weakening connection points so that striped patterns appear at the connection points.

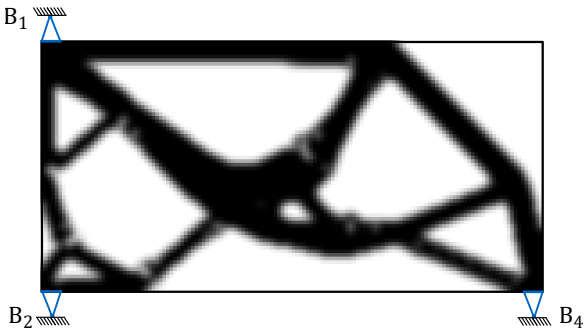

(a) Optimized topology with three bolts.

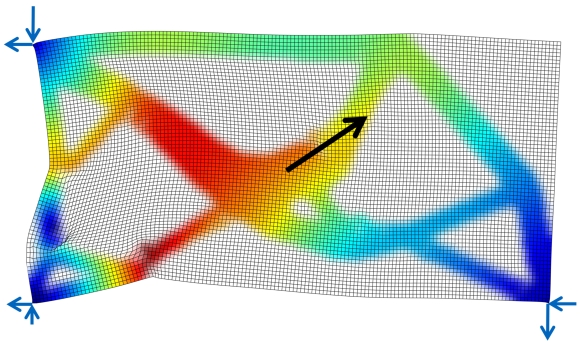

(b) Deformed shape, external force for load case 2, and $F_{lp,n}$ and $F_{lp,t}$.

Figure 7: Three-bolt variant: the joint load constraint can be met with one fewer bolt, aided by a compliant load path.

5 DISCUSSION

The examples show that the proposed constraint is effective in reducing joint loads. For low friction coefficients μ, shear has a strong impact on the required preload. The optimizer then steers the design to reduce shear at the joints and accept more normal load.
The constraint also enables a reduction in the number of joints while satisfying the limit $F_{M,c}$. In doing so, the optimizer may form compliant mechanisms [23], which can reduce joint loads substantially but also increase structural compliance. For many engineering applications that use bolted joints, such flexibility is undesirable.
The constraint is easy to implement, with low FE modeling effort of the joint, the interface, and the structure.
The method can be used for various applications. The constraint g_k can be adapted to impose lower and upper bounds, to target specific force components, or to regulate interface forces under a prescribed actuator input.
The constraint is computationally inexpensive: in addition to the standard state solve, one adjoint linear system (17) per joint constraint is required. However, for compliant mechanism synthesis, many iterations might necessary to convergence.
Finally, the assumption $\phi = 0$ is only reasonable under certain conditions. The allowable preload $F_{M,c}$ should be selected with care and optimized structures should be verified with detailed FE models.

6 CONCLUSION AND OUTLOOK

This study adds a joint load constraint for TO and derives adjoint sensitivities for efficient computation. The bolt is modeled according to VDI 2230 model class I. The joint itself is not represented in the FE. Only the required preload is approximated from interface loads so that sliding and joint opening are avoided for combined normal and shear loads.
Numerical results show that, especially for low friction coefficients, the constraint simultaneously lowers joint loads across all bolts by routing loads more normal and reducing shear. The constraint can also support to reduce the number of joints. Large reductions may be realized via the creation of compliant mechanisms, which can be impractical when a stiff structure is required.
As an outlook, additional failure modes can be incorporated (e.g., one-sided opening due to eccentric loading) and the method can be extended to 3D, where torsional effects matter. Preload can also be included directly in the FE model with modest changes to the constraint and sensitivity derivations, allowing a more realistic representation of the assembled joint. Constraining interface loads, either by upper or lower limits, may be useful in other applications, such as compliant mechanism synthesis.

ACKNOWLEDGEMENTS

The authors acknowledge the support from the Federal Ministry for Economic Affairs and Climate Action (BMWK) of the Federal Republic of Germany, which provided funding for this project under project number AZ-1625-24. The results, opinions and conclusions expressed in this publication are those of the authors and do not necessarily reflect the views of AUDI AG.

REFERENCES

[1] Ji-Hong Zhu, Wei-Hong Zhang, and Liang Xia. “Topology Optimization in Aircraft and Aerospace Structures Design”. In: *Archives of Computational Methods in Engineering* 23.4 (Dec. 1, 2016), pp. 595–622. ISSN: 1886-1784. DOI: 10.1007/s11831-015-9151-2.

[2] Li Peng et al. “Topology optimization methods and its applications in aerospace: a review: L. Peng et al.” In: *Structural and Multidisciplinary Optimization* 68.5 (2025), p. 105. DOI: 10.1007/s00158-025-04030-x.

[3] Ronald Bartz et al. “Density-based shape optimization of 3D structures with mean curvature constraints”. In: *Structural and Multidisciplinary Optimization* 65.1 (Jan. 2022), p. 5. ISSN: 1615-147X, 1615-1488. DOI: 10.1007/s00158-021-03089-6.

[4] Fabian Duddeck et al. “Topology optimization for crashworthiness of thin-walled structures under axial impact using hybrid cellular automata”. In: *Structural and Multidisciplinary Optimization* 54.3 (2016), pp. 415–428. DOI: 10.1007/s00158-016-1445-y.

[5] Martin P. Bendsøe and Ole Sigmund. *Extensions and applications*. Ed. by Martin P. Bendsøe and Ole Sigmund. Berlin, Heidelberg: Springer, 2004, pp. 71–158. ISBN: 978-3-662-05086-6. DOI: 10.1007/978-3-662-05086-6_2.

[6] Felix Endress, Jasper Rieser, and Markus Zimmermann. “On the treatment of requirements in DfAM: three industrial use cases”. In: *Proceedings of the Design Society* 3 (2023), pp. 2815–2824.

[7] Martin Philip Bendsøe and Noboru Kikuchi. “Generating optimal topologies in structural design using a homogenization method”. In: *Computer methods in applied mechanics and engineering* 71.2 (1988), pp. 197–224.

[8] Joshua D Deaton and Ramana V Grandhi. “A survey of structural and multidisciplinary continuum topology optimization: post 2000”. In: *Structural and multidisciplinary optimization* 49.1 (2014), pp. 1–38.

[9] Christoph Klahn et al. “Entwicklung und konstruktion für die additive fertigung”. In: *Grundlagen und Methoden für den Einsatz in industriellen Endkundenprodukten* 1 (2018).

[10] ZHU Jihong et al. “A review of topology optimization for additive manufacturing: Status and challenges”. In: *Chinese Journal of Aeronautics* 34.1 (2021), pp. 91–110.

[11] Karl-Hein Kloos and Wolfgang Thomala. *Schraubenverbindungen*. Springer, 2007.

[12] Tobias Wanninger, Jintin Frank, and Markus Zimmermann. “Topology optimisation of multiple robot links considering screw connections”. In: *Proceedings of the Design Society* 4 (May 2024), pp. 1879–1888. ISSN: 2732-527X. DOI: 10.1017/pds.2024.190.

[13] Olaf Ambrozkiewicz and Benedikt Kriegesmann. “Simultaneous topology and fastener layout optimization of assemblies considering joint failure”. In: *International Journal for Numerical Methods in Engineering* 122.1 (Jan. 15, 2021), pp. 294–319. ISSN: 0029-5981, 1097-0207. DOI: 10.1002/nme.6538.

[14] Johan Ekh and Joakim Schön. “Finite element modeling and optimization of load transfer in multi-fastener joints using structural elements”. In: *Composite Structures* 82.2 (Jan. 1, 2008), pp. 245–256. ISSN: 0263-8223. DOI: 10.1016/j.compstruct.2007.01.005.

[15] H. Chickermance et al. “Optimal fastener pattern design considering bearing loads”. In: *Structural optimization* 17.2 (Apr. 1, 1999), pp. 140–146. ISSN: 1615-1488. DOI: 10.1007/BF01195938.

[16] Ji-Hong Zhu et al. “Structural topology optimization with constraints on multi-fastener joint loads”. In: *Structural and Multidisciplinary Optimization* 50.4 (Oct. 2014), pp. 561–571. ISSN: 1615-147X, 1615-1488. DOI: 10.1007/s00158-014-1071-5.

[17] *VDI 2230 Blatt 2 - Systematische Berechnung hochbeanspruchter Schraubenverbindungen - Mehrschraubenverbindungen*. Dec. 2014.

[18] Erik Andreassen et al. “Efficient topology optimization in MATLAB using 88 lines of code”. In: *Structural and Multidisciplinary Optimization* 43.1 (2011), pp. 1–16.

[19] *VDI 2230 Blatt 1 - Systematische Berechnung hochbeanspruchter Schraubenverbindungen - Zylindrische Einschraubenverbindungen*. Nov. 2015.

[20] Ole Sigmund. "On benchmarking and good scientific practise in topology optimization". In: *Structural and Multidisciplinary Optimization* 65.11 (Nov. 2022), p. 315. ISSN: 1615-147X, 1615-1488. DOI: 10.1007/s00158-022-03427-2.

[21] Johannes Soika et al. "A procedure model to manage requirements for topology optimization and additive manufacturing". In: *Proceedings of the Design Society* 5 (Aug. 2025), pp. 229–238. ISSN: 2732-527X. DOI: 10.1017/pds.2025.10037.

[22] Krister Svanberg. "The method of moving asymptotes—a new method for structural optimization". In: *International journal for numerical methods in engineering* 24.2 (1987), pp. 359–373. DOI: 10.1002/nme.1620240207.

[23] Ole Sigmund. "On the design of compliant mechanisms using topology optimization". In: *Journal of Structural Mechanics* 25.4 (1997), pp. 493–524. DOI: 10.1080/08905459708945415.